Automotive Science and Engineering, Vol. 15, No. 4, (2025), 4864-4870

Iran University of Science and Technology

Automotive Science and Engineering

Journal Homepage: ase.iust.ac.ir

ISSN: 2008-9899

RD-CFAR: Fast and Accurate Constant False Alarm Rate Algorithm for Automotive Radar Application

Jamal Kazaz[1*], Mahmoud Kamarei[2], Mohammad Fakharzadeh[3]

[1,2] University of Tehran, Tehran, Iran.

[3] Sharif University of Technology

ARTICLE INFO

Article history:
Received : 18 Jan 2025
Accepted: 29 Sep 2025
Published: 19 Oct 2025

Keywords:
automotive radar
Constant False Alarm Rate (CFAR)
interfering target
Range-Doppler map
target detection

A B S T R A C T

Target detection using cameras or automotive radar to identify traffic or prevent collisions is an important issue in Autonomous Vehicles (AV) research. Traditional Constant False Alarm Rate (CFAR) methods are commonly employed. Although these methods are suitable for lightweight hardware, improving the target detection process often leads to losing real-time performance. The method proposed in this paper improves detection accuracy. It reduces response time by modifying the position of guard cells in the first stage and employing harmonic averaging (inverse of the sum of the inverse of data) while eliminating data sorting in the second stage. Moreover, this approach exhibits better performance in the presence of interfering targets. Since the proposed method is more applicable to the Range-Doppler map, it has been named RD-CFAR. The proposed method also enhances target detection in Synthetic Aperture Radar (SAR) images. Simulation results demonstrate that the proposed algorithm improves detection probability by nearly 40% compared to conventional methods (like CA-CFAR), while maintaining comparable computational time.

1. Introduction

AUTONOMOUS vehicles (AV) represent one of the most innovative technologies of this century, holding a unique position in scientific and industrial research. A combination of different techniques and technologies such as artificial intelligence, advanced sensors, and data processing algorithms are integrated in AV to improve transportation for both humans and goods [1]. Autonomous vehicles can significantly contribute to reducing accidents, improving transportation efficiency, and minimizing environmental impacts, thereby paving the way for a more sustainable future.

One of the critical challenges in the development of autonomous vehicles is the precise and fast detection of targets in the surrounding environment, which is achieved using sensory systems such as cameras, radars, and LIDARs, with their advantages and limitations. While cameras provide high-resolution visual data, radars perform better in adverse weather conditions, such as fog or rain. The fusion of these sensor data and the application of advanced algorithms, such as deep learning, have significantly enhanced target detection and tracking accuracy [2]-[4].

Automotive radars, as one of the most essential sensors in autonomous vehicles, play a vital role in detecting and tracking targets by transmitting and receiving radio waves to extract information such as distance, velocity, and direction of objects.

Nevertheless, radar performance can be impacted by factors such as wave interferences, which degrade the system's accuracy and safety

*Corresponding Author
Email Address: Jamal.kazazi@ut.ac.ir
https://doi.org/10.22068/ase.2025.711

[DOI: 10.22068/ase.2025.711]

[5]. Understanding the types of interference in automotive radars, their impacts, and methods to mitigate them are crucial research topics in this field. In current commercial AV, multiple sensors are typically deployed to ensure robust perception. Among these sensors, radar occupies a particularly prominent role due to its resilience in adverse weather conditions and cluttered environments [1-5].

CFAR (Constant False Alarm Rate) methods are standard algorithms used for target detection in the presence of noise, clutter, and interference. These algorithms maintain a constant rate of false alarms, ensuring optimal performance across different environments. Among CFAR variants, Cell Averaging (CA-) CFAR is one of the most efficient and commonly used methods, determining the detection threshold based on the mean signal power within a reference window [6]. While effective in environments with uniform noise distribution, the performance of CA-CFAR degrades in the presence of strong signals/interference due to elevated thresholds.

To address these limitations, advanced CFAR methods have been developed. Ordered Statistics (OS-) CFAR, for example, sets the threshold using a specific order statistic, such as the median, which performs better than OS-CFAR in non-uniform noise environments or when multiple closely spaced targets exist [9]. OSS-CFAR optimizes OS-CFAR by reducing the number of sorted data, thereby enhancing computational efficiency [10]. Trimmed-Mean (TM-) CFAR excludes the highest and lowest samples in the reference window and calculates the threshold based on the remaining samples [11]. Similarly, Weighted Amplitude Iteration (WAI-) CFAR applies iterative weighted averaging, though at the cost of higher computational complexity [12]. Censored Harmonic Averaging (CHA-)CFAR further improves detection accuracy by combining harmonic averaging and OS-CFAR principles [13].

The proposed Range-Doppler (RD-) CFAR method introduces a novel approach by modifying the guard cell configuration and eliminating data sorting, achieving a faster response time while maintaining high detection accuracy.

2. Proposed Algorithm

The objective of the proposed algorithm is to enhance target detection performance in automotive radars, specifically for RD maps generated using two stages of Fast Fourier Transforms (FFT). In practical applications, the FFT is often computed with $2^{m_1} \times 2^{m_2}$points, where m_1, m_2 are typically 8, 9, or 10.

Therefore, the data points in the RD map are always divisible by 4. The general structure of such a map is shown in Figure 1, where each target appears in a certain row and column. This characteristic can elevate the estimated noise threshold in traditional CFAR algorithms.

Given the commercial nature of automotive radars, an ideal algorithm should achieve an acceptable detection accuracy with minimal computational complexity and fast response time. Automotive radars are designed to prevent collisions and traffic congestion, which necessitates fast target detection processes, ideally with minimal hardware requirements.

The RD-CFAR algorithm incorporates two main improvements. To reduce noise level estimation errors, the shape of the guard cells surrounding a target is altered. These cells are not considered in threshold finding calculations. Besides excluding the immediate neighboring cells in a square configuration $N_G \times N_G$,

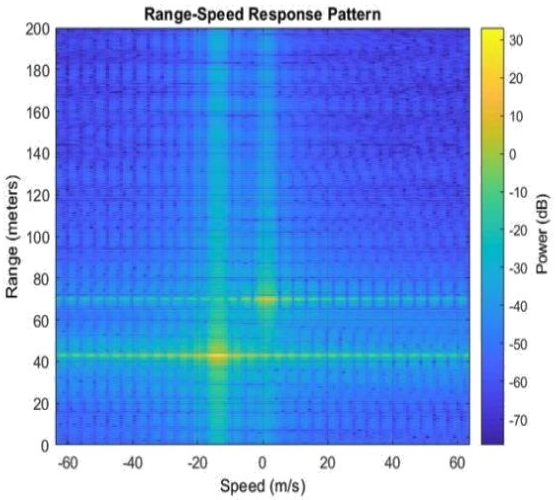

Figure 1: RD map of two targets in front of an automotive radar

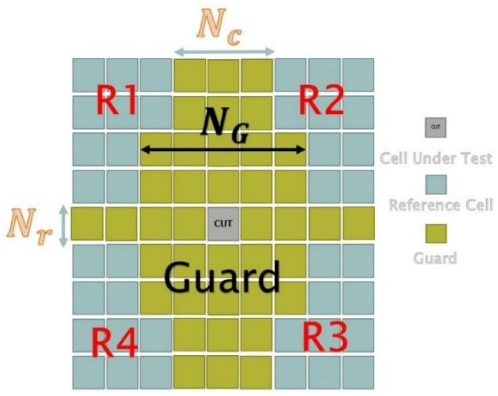

Figure 2: Windows of the proposed CFAR Algorithm

[DOI: 10.22068/ase.2025.711]

additional N_r rows and N_C columns adjacent to the target cell are omitted from calculations. Figure 2 illustrates the modified guard cells. On the other hand, traditional algorithms such as OS-CFAR rely on sorting the data, while CHA-CFAR requires harmonic averaging, both of which are computationally expensive. The proposed algorithm avoids sorting and minimizes harmonic averaging, reducing computational complexity. Instead, the algorithm divides the data into four groups, computes the sum for each group, and finally determines the harmonic mean of the four sums for threshold comparison. A comparison of these methods is presented in Table 1.

Tabel 1: Comparison of CFAR Methods

Method	Sort	Inverse	Guard Cells	Level Estimator
CA-CFAR	No	No	$N_r = N_c = 0$ $N_G \neq 0$	$g = \sum_{n=1}^{N} x_i$
TM-CFAR	All data	No	$N_r = N_c = 0$ $N_G \neq 0$	$g = \sum_{k=N_1}^{N_2} x_{(k)}$
OS-CFAR	All data	No	$N_r = N_c = 0$ $N_G \neq 0$	$g = x_{(k)}$
OSS-CFAR	All Groups	No	$N_r = 1$ $N_c = 1$ $N_G = 0$	$y_i = \sum x_{ij}$ $g = y_{(k)}$
WAI-CFAR	No Iteration	No Iteration	$N_r = N_c = 0$ $N_G \neq 0$	See [12] for details
CHA-CFAR	All data	$N - N_1 + 1$	$N_r = N_c = 0$ $N_G \neq 0$	$g = \frac{1}{\sum_{k=N_1}^{N} \frac{1}{x_{(k)}}}$
RD-CFAR	No	5	$N_r \neq 1$ $N_c \neq 1$ $N_G \neq 0$	$g = \frac{1}{\sum_{j=1}^{4} \frac{1}{y_j}}$ $Y_j = \sum_{i=1+(j-1)\times\frac{N}{4}}^{j\times\frac{N}{4}} X_i$ $j = 1,2,3,4$

In scenarios with N-independent targets in an RD map, N^2-N ghost targets can potentially arise due to interference between targets [14]. By removing potential interfering points, the accuracy of noise threshold estimation inherently improves. Figure 3 further illustrates the degradation in detection accuracy caused by interfering targets within the noise and clutter calculation window. The more cells with a high probability of containing a strong signal or being dependent on it are excluded from the calculations, the better the performance will be.

3. Detection Probability Formulation

Following the modification of guard cells, the *N=4M* data points are grouped into four regions, and a sum is computed for each region. The harmonic mean of these four sums serves as the thresholds for comparison:

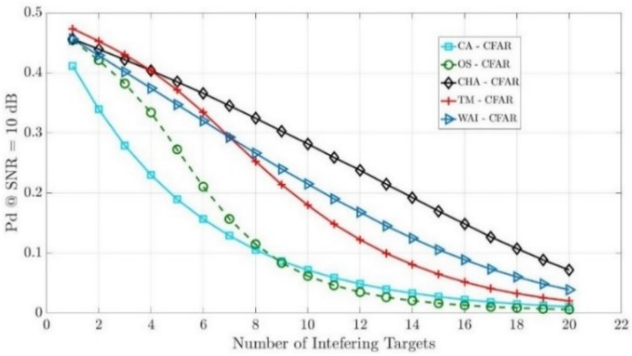

Figure 3: different CFAR methods' performance when number of interfering target changes

$$Y_j = \sum_{i=1+(j-1)\times M}^{j\times M} X_i \quad j = 1,2,3,4 \qquad (1)$$

Assuming the independence of X_i and their exponential distribution with the parameter $\lambda = 1$ [10], [13], the probability density function (PDF) of Y_j, which represents the sum of exponentially distributed random variables with identical parameters will follow a Gamma distribution [15]:

$$f_{Y_j}(y) = \frac{1}{(M-1)!} y^{M-1} e^{-y} \quad y > 0 \qquad (2)$$

Now, for the four obtained data points, there are several approaches. First, the data can be sorted using methods such as OS-CFAR and CHA-CFAR, followed by selecting among sorted data. Alternatively, all four data points can be included in the calculation process. This paper proposes the Z function in the form of the harmonic mean of the four data points, similar to what was done in [13] for a subset of sorted data points:

$$W_j = \frac{1}{Y_j} \rightarrow W = \sum_{j=1}^{4} W_j \rightarrow Z = \frac{1}{W} \qquad (3)$$

[DOI: 10.22068/ase.2025.711]

In this approach, there is no need for sorting. This is because each data point is an output of a summation and the differences between these four data points. In the simulation part, first, the data will be sorted and will be shown that the best performance is when all data are considered. (See Figure 4 for details). Consequently, the computational complexity inherent in other methods is naturally reduced. For the probability density of the random variable W, the theory of "function of a random variable" is applied [16], therefore:

$$\begin{aligned} f_{W_j}(\omega) &= \omega^{-2} f_{Y_j}(\omega^{-1}) \\ &= \frac{1}{(M-1)!}\omega^{-2}\frac{1}{\omega^{N-1}}e^{-\frac{1}{\omega}} \\ &= \frac{1}{(M-1)!}\frac{1}{\omega^{M+1}}e^{-\frac{1}{\omega}} \end{aligned} \quad (4)$$

On the other hand, considering the relationship between W and W_j, the moment-generating functions (MGF) of these two random variables are related as follows [16]:

$$\begin{aligned} I &= \Phi_{W_j}(s) \\ &= \int_0^{\infty} \frac{1}{(M-1)!}\frac{1}{\omega^{M+1}}e^{-\frac{1}{\omega}}e^{s\omega}d\omega \end{aligned} \quad (5)$$

$$W = \sum_{j=1}^{4} W_j \Longrightarrow \Phi_W(s) = \Phi_{W_j}^4(s) \quad (6)$$

Using integral tables and Wolfram Mathematica [17], the integral I is expressed in the following closed form:

$$I = 2\sqrt{(-s)^M}\frac{K_M\left(2\sqrt{-s}\right)}{(N-1)!} \qquad Re\{s\} < 0 \quad (7)$$

where $K_M(.)$ is the modified Bessel function of the second kind, also known as the Kelvin function. This problem can also be solved using complex contour integration and the residue theorem; however, solving it in this manner is beyond the scope of this paper, and therefore only the final result has been presented. Furthermore, as stated in [18], since Z is inversely related to W it follows that:

$$\begin{aligned} &\int_0^{\infty} \frac{1}{x^2} f_X\left(\frac{1}{x}\right) e^{sx}\, dx \\ &= \int_{-s}^{\infty}\int_0^{\infty} J_0\left(2\sqrt{\mu\alpha}\right)\Phi_X(-\alpha)\, d\alpha d\mu \end{aligned} \quad (8)$$

$$\begin{aligned} &\Phi_z(s) \\ &= \int_{-s}^{\infty}\int_0^{\infty} J_0\left(2\sqrt{\mu\alpha}\right)\left(2\sqrt{\alpha^M}\frac{K_M\left(2\sqrt{\alpha}\right)}{(N-1)!}\right)^4 d\alpha d\mu \end{aligned} \quad (9)$$

where $J_0(.)$ is the Bessel function of the first kind of order zero. Finally, the false alarm probability is given by:

$$\begin{aligned} P_{fa} &= Pr\{X_{CUT} \geq \tau Z\} \\ &= \int_0^{\infty} Pr\{X_{CUT} \geq \tau Z | Z = \eta\} f_Z(\eta) d\eta \end{aligned} \quad (10)$$

Since the occurrence of X_{CUT} follows an exponential distribution with parameter λ, by substituting the exponential probability distribution formula, the desired probability is obtained as follows:

$$\begin{aligned} \Pr\{X_{CUT} \geq \tau Z | Z = \eta\} &= 1 - F_X(\tau\eta) \\ &= 1 - \left(1 - e^{-\tau\lambda\eta}\right) \\ &= e^{-\tau\lambda\eta} \end{aligned} \quad (11)$$

therefore:

$$P_{fa} = \int_0^{\infty} e^{-\tau\lambda\eta} f_Z(\eta) d\eta = \Phi_z(-\tau\lambda) \quad (12)$$

By plotting the graph of $\Phi_z(.)$, the threshold for comparison in this algorithm can be determined. To enhance readers' understanding of the behavior of this function, it is worth noting that the value of $\Phi_z(x)$ at −20 is 0.0048, while at −10 it is 0.0156.

4. Simulation and Results

Taking into account both of the described improvements, the simulation was performed using MATLAB to evaluate its performance. First, the guard cells were modified as shown in Figure 2 for all methods. Cells that were left out could act as interfering targets if present, causing an increase in noise and clutter levels around them, as seen earlier in Figure 3. Therefore, it is evident that even if the noise and clutter level calculation function remain unchanged, removing cells that are likely to contain targets improves detection probability in all algorithms.

Next, assuming a fixed false alarm rate and identical guard cells for all, the performance of different algorithms was compared with the proposed method. First, the Y_j's are sorted to

[DOI: 10.22068/ase.2025.711]

examine whether sorting is necessary. Figure 4 shows the detection probability using this algorithm for different numbers of selected data from 4 sorted data, assuming the same false alarm rate. In this graph, the results for *fourCHA(i)* represent the use of sorted data points numbered (i) through (4) in the calculations. As shown in the graph, the presence of all 4 data points in the calculations results in better performance. In this simulation, for signal to noise and clutter ratio (SNCR) ranging from −5 to 40 dB with a step of 2 dB, one million data points were tested with each method in every run.

This simulation was conducted with data similar to automotive radar data. In addition, the calculation window was assumed to be as shown in Figure 2. In this window, two targets with a specified SNCR, which reflection of their magnitude, are placed in cells with the same row or column, with clutter accumulated by the *sinc(.)* function. Figure 5 displays a sample of the test scenarios. In this figure, the main target is located at (4,4), while two interfering targets are positioned at (1,2) and (6,7). As shown in Figure 4, utilizing all four data points and the proposed method (represented by the pink curve with triangular markers) outperforms all traditional methods. However, its performance in target detection is lower than CHA-CFAR and WAI-CFAR. This is because, in CHA-CFAR, all data points are sorted, and most undergo inversion. Similarly, in WAI-CFAR, an iterative relation is used, making both methods computationally complex and requiring significantly more operations than the proposed method. Consequently, for applications requiring faster processing or computations on less powerful hardware (e.g., commercial automotive radar), the proposed method in this paper demonstrates better performance.

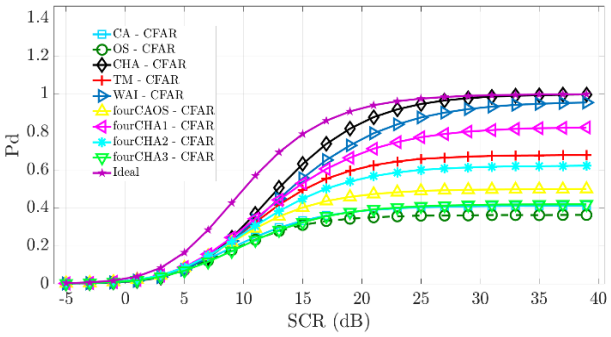

Figure 4: Performance of different CFAR methods.

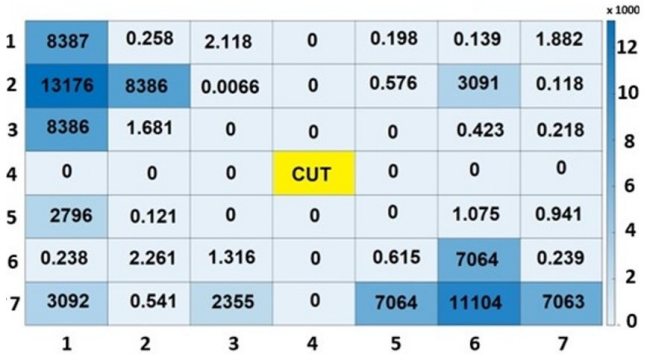

Figure 5: Sample of test Scenarios. 10^6 scenarios were tested for each SNCR

To illustrate this, Figure 6 presents the time required for target detection using different CFAR methods based on the number of data points involved in the calculations. As seen in Figure 6, the WAI-CFAR method performs poorly in terms of response speed, deviating significantly from other methods. After excluding WAI-CFAR from the comparison, the proposed method demonstrates better performance than CHA-CFAR, TM-CFAR, and OS-CFAR. Its response speed is comparable to CA-CFAR, while its detection performance, as shown in Figure 4, surpasses that of TM-CFAR and OS-CFAR.

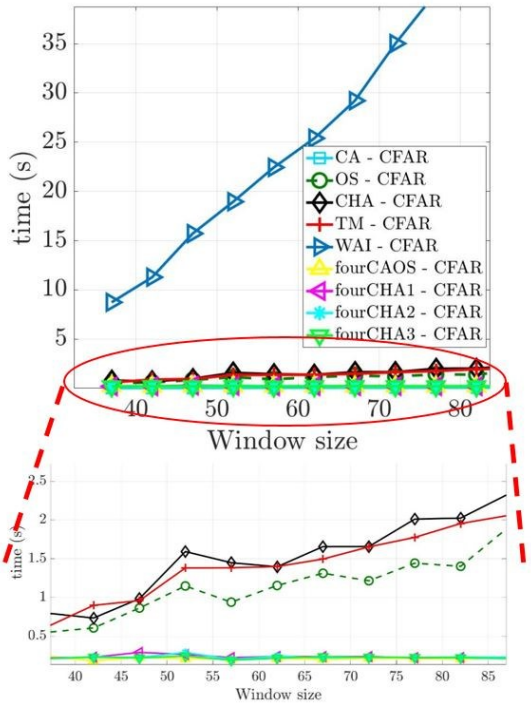

Figure 6: The time required for target detection in different CFAR methods based on the window size. The CPU was Intel(R) Core (TM) i7-7500U.

[DOI: 10.22068/ase.2025.711]

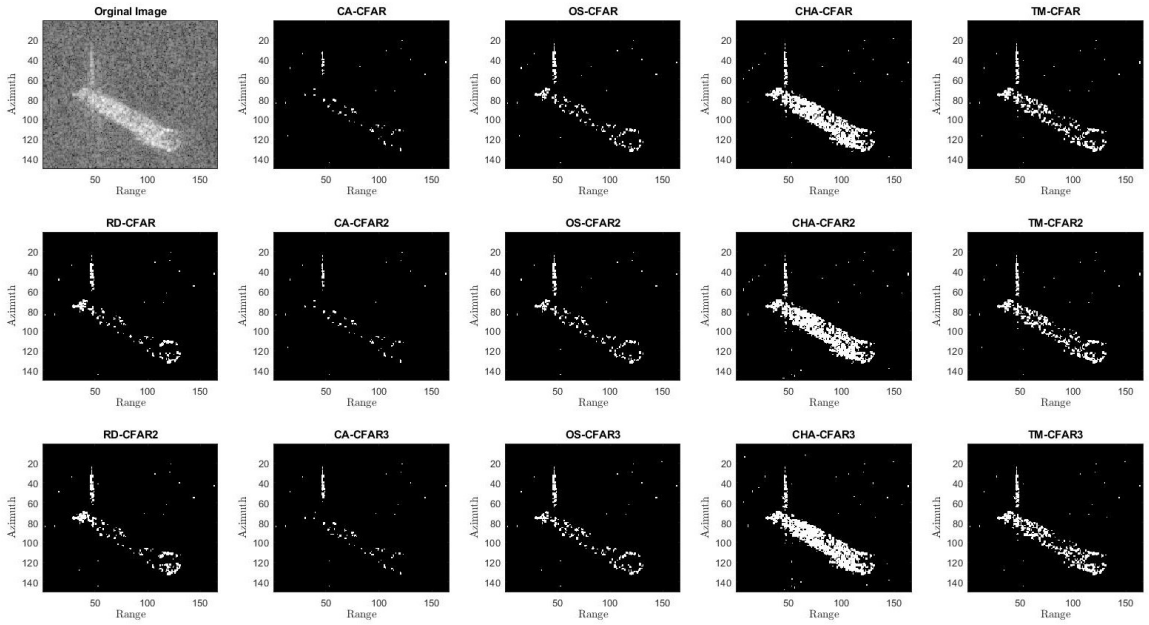

Figure 7: Performance of different CFAR methods for detecting targets in SAR images. For pictures in first row, traditional guard cells were used. In the pictures in the second row, $N_r = N_c = 1$, and in the last row, $N_r = N_c = 3$.

Subsequently, leveraging [13], the performance of this method, referred to as RD-CFAR, was evaluated for target detection in Synthetic Aperture Radar (SAR) images. Figure 7. illustrates the performance of different methods for target detection in SAR images. The first row represents target detection using the traditional guard cell configuration. The second row assesses various methods, including the proposed method, with adjusted guard cells set to $N_r = N_c = 1$. The third row evaluates all methods with modified guard cells set to $N_r = N_c = 3$.

As observed in the figure, the proposed method outperforms comparable methods. Improvements in other methods due to the modified guard cell configuration are also evident. Regarding to RD-CFAR level estimator, choosing a smaller size of the calculation window, making the performance of this method closer to CHA-CFAR. Conversely, as the calculation window includes more data, the proposed method approaches the performance of CA-CFAR and its derivatives due to the superiority of summation operations over inversion. Therefore, this method is more suitable for smaller windows.

The originality of the modified guard cell structure stems from the row-column dependency of the data. Naturally, in SAR images target detection, where target points are not necessarily aligned along rows and columns and may appear diagonally, the results are not as effective as those derived from automotive radar RD maps. The parameters N_r and N_c in this structure can be adjusted to accommodate larger targets, such as ships shown in Figure 7, and for various applications.

5. Conclusions

This paper proposed a novel CFAR method for target detection in automotive radars. The method initially modifies the guard cell configuration and then introduces an innovative approach that delivers acceptable performance with faster response time. The formulation of target detection probability, testing of the method in the presence of interfering targets, and evaluation of the method for target detection in SAR images were derived in this paper. The use of this modification in AV can provide real-time responsiveness while enhancing target detection in foggy or high-clutter environments.

References

[1] S. Thrun, "Toward robotic cars," Communications of the ACM, vol. 53, no. 4, (2010), pp. 99-106.

[2] F. J. Abdu, Y. Zhang, M. Fu, Y. Li, and Z. Deng, "Application of Deep Learning on Millimeter-Wave Radar Signals: A Review," Sensors, vol. 21, no. 6, (2021), p. 1951. [Online]. doi: https://doi.org/10.3390/s21061951

[DOI: 10.22068/ase.2025.711]

[3] J. Kazazi, A. Mahdavi, M. Kamarei, and M. Fakharzadeh, "Automotive Radar Simulator Based on Ray-Tracing and Machine Learning," in Proc. 11th Int. Symp. on Telecommunications (IST), Tehran, Iran, (2024).

[4] J. Kazazi, S. M. M. AleMohammad, and M. Kamarei, "U-Net-Based Automotive Radar Target Detection and Recognition," in Proc. 32nd Int. Conf. on Electrical Engineering (ICEE), Tehran, Iran, (2024), pp. 1-5, doi: 10.1109/ICEE63041.2024.10667698.

[5] M. Ritchie et al., "Interference mitigation for automotive radar using orthogonal noise waveforms," IEEE Trans. Vehicular Technology, vol. 63, no. 1, (2014), pp. 45-59.

[6] P. Gandhi and S. Kassam, "Optimality of the cell averaging CFAR detector," IEEE Trans. Inf. Theory, vol. 40, no. 4, (1994), pp. 1226-1228.

[7] M. Weiss, "Analysis of some modified cell-averaging CFAR processors in multiple-target situations," IEEE Trans. Aerosp. Electron. Systems, vol. AES-18, no. 1, (1982), pp. 102–114.

[8] V. G. Hansen and J. H. Sawyers, "Detectability loss due to 'greatest of' selection in a cell-averaging CFAR," IEEE Trans. Aerosp. Electron. Syst., vol. AES-16, no. 1, pp. 115–118, Jan. 1980.

[9] H. Rohling, "Radar CFAR thresholding in clutter and multiple target situations," IEEE Trans. on Aerospace and Elect. Syst., no. 4, (1983), pp. 608–621.

[10] T. Jeong, S. Park, J. -W. Kim, and J. -W. Yu, "Robust CFAR Detector With Ordered Statistic of Sub-Reference Cells in Multiple Target Situations," IEEE Access, vol. 10, (2022), pp. 42750-42761, doi: 10.1109/ACCESS.2022.3168707.

[11] P. P. Gandhi and S.A. Kassam, "Analysis of CFAR processors in nonhomogeneous background," IEEE Trans. on Aerospace and Electronic Systems, vol. 24, no. 4, (1988), pp. 427–445.

[12] W. Zhou, J. Xie, G. Li, and Y. Du, "Robust CFAR detector with weighted amplitude iteration in nonhomogeneous sea clutter," IEEE Trans. on Aerospace and Electronic Systems, vol. 53, no. 3, (2017), pp. 1520–1535.

[13] R. G. Zefreh, M. R. Taban, M. M. Naghsh, and S. Gazor, "Robust CFAR Detector Based on Censored Harmonic Averaging in Heterogeneous Clutter," IEEE Trans. on Aerospace and Electronic Systems, vol. 57, no. 3, (2021), pp. 1956-1963, doi: 10.1109/TAES.2020.3046050.

[14] H. Zhou, P. Cao, and S. Chen, "A novel waveform design for multi-target detection in automotive FMCW radar," in 2016 IEEE Radar Conference (RadarConf), Philadelphia, PA, USA, (2016), pp. 1-5, doi: 10.1109/RADAR.2016.7485315.

[15] G. M. Dillard, "Mean-Level Detection of Nonfluctuating Signals," IEEE Trans. on Aerospace and Electronic Systems, vol. AES-10, no. 6, (1974), pp. 795-799, doi: 10.1109/TAES.1974.307886.

[16] A. Papoulis and S. U. Pillai, Probability, Random Variables, and Stochastic Processes, 4th ed. New York, NY, USA: McGraw-Hill Europe, (2002).

[17] Wolfram Research, Inc., Mathematica Online, Champaign, IL, USA: Wolfram Research, Inc. [Online]. Available: https://www.wolfram.com/mathematica/online/, [Accessed: Jan. 2025].

[18] A. Prudnikov, Y. A. Brychkov, and O. Marichev, Integrals and Series: Direct Laplace Transforms, vol. 4, Boca Raton: CRC, (1992).

[DOI: 10.22068/ase.2025.711]